Non-linear dynamics of the double tearing mode

E. Nardon,[1] V. Bandaru,[2, a)] M. Hoelzl,[2] F.J. Artola,[3] P. Maget,[1] the JOREK team,[4] and JET contributors[5]
[1)] *CEA, IRFM, F-13108 Saint-Paul-lez-Durance, France*
[2)] *Max Planck Institute for Plasma Physics, Boltzmannstr. 2, 85748 Garching b. M., Germany*
[3)] *ITER Organization, Route de Vinon sur Verdon, 13115 St Paul Lez Durance, France*
[4)] *See the author list of M. Hoelzl et al. 2021 Nucl. Fusion 61 065001*
[5)] *See the author list of 'Overview of JET results for optimising ITER operation' by J. Mailloux et al. 2022 Nucl. Fusion 62 042026*

(*Electronic mail: eric.nardon@cea.fr)

(Dated: 1 September 2023)

3D non-linear magnetohydrodynamics simulations of a double tearing mode with the JOREK code are presented in the context of trying to better understand the benign termination of runaway electron beams observed in some experiments. It is shown that the non-linear behaviour qualitatively depends on the resistivity η *via* its effect on how fast secondary, non-linearly destabilized, tearing modes grow relative to the primary mode. Within a certain range of η, a violent and global relaxation is observed, consistent with the 'Kadomtsev-predicted' reconnection region extending from almost the very centre up to the edge of the plasma.

I. INTRODUCTION

The double tearing mode (DTM)[1,2] has been studied by several authors using non-linear magnetohydrodynamics (MHD) simulations, in connection with the topic of fast reconnection[3]. Most studies have used 2D simulations assuming helical symmetry[4–9]. The DTM was found to display, in some regions of parameter space, an 'explosive' non-linear behaviour leading to a violent relaxation. In the present paper, we investigate the non-linear dynamics of the DTM in 3D using the JOREK code. A key difference between 2D and 3D simulations is that in 3D, modes of various helicities are involved, allowing magnetic stochasticity to appear, which is not possible in 2D. We note that 3D simulations of the DTM have been published previously, but with a different focus compared to the present paper[10,11]. In particular, here we use a setup derived from a study on the benign termination of Runaway Electron (RE) beams in JET[12,13] for which (as we will show) the reconnected region predicted by the Kadomtsev model[10] extends from almost the very centre up to the edge of the plasma. This contrasts with Refs. 10 and 11 where the 'Kadomtsev-predicted' reconnection region does not (by far) extend up to the edge (see Fig. 13 in Ref. 10) and where, consistently, simulations produce a partial rather than global (in terms of radial extent) relaxation. Also, a particular focus of the present study is the role of the resistivity η in the non-linear dynamics, which is not addressed in Refs. 10 and 11.

Consistently with the Kadomtsev model prediction, we observe a global and violent relaxation resulting in an almost complete flattening of the current density profile at fixed magnetic helicity. However, this is only the case within a certain range of η, which corresponds to electron temperatures between $\simeq$ 13 and 47 eV when using the Spitzer resistivity expression[14]. Outside this range, the behaviour is qualitatively different and such a violent relaxation is not observed. Our aims here are 1) to describe the violent relaxation and 2) to investigate the cause for the η dependence of the non-linear behaviour.

The paper is constructed as follows. Section II describes the model and the simulation setup. Section III focuses on the violent relaxation. Section IV discusses the dependence of the non-linear dynamics on η. Finally, Section V summarizes the results and discusses their implications.

II. MODEL AND SIMULATION SETUP

For this study, the JOREK code[15,16] is used with a pressureless reduced MHD model which ignores parallel flows, and where a constant and flat electron density $n_e = 10^{19}$ m^{-3}, resulting in a mass density $\rho = m_D n_e = 3.3 \cdot 10^{-8}$ kg/m^3 (m_D being the mass of deuterium), is imposed. The code evolves the poloidal flux ψ and the electric potential u (which is also the flow potential) in 3D toroidal (R,Z,ϕ) geometry, according to the following normalized equations:

$$\frac{\partial \psi}{\partial t} = R[\psi,u] - F_0 \frac{\partial u}{\partial \phi} + \eta (j_\phi - j_{\phi 0}) \tag{1}$$

$$\nabla \cdot \left[R^2 \rho \nabla_{pol} \frac{\partial u}{\partial t} \right] = \frac{1}{R}[R^4 \rho \omega, u] - \frac{1}{2R}[R^2 \rho, R^2 |\nabla_{pol} u|^2] + \frac{1}{R}[\psi, j_\phi] - \frac{F_0}{R^2}\frac{\partial j_\phi}{\partial \phi} + \mu \Delta \omega \tag{2}$$

where $j_\phi \equiv \Delta^* \psi \equiv R^2 \nabla \cdot (\frac{1}{R^2} \nabla_{pol} \psi)$ is the toroidal current density and $\omega \equiv \Delta_{pol} u \equiv \nabla \cdot \nabla_{pol} u$ is the toroidal vorticity, with ∇_{pol} the gradient in the poloidal (R,Z) plane. $j_{\phi 0}$ is the initial value of j_ϕ, and η and μ are the resistivity and viscosity, which are constant in time and space. The Poisson brackets are defined as follows: $[A,B] \equiv \mathbf{e}_\phi \cdot (\nabla A \times \nabla B)$, where $\mathbf{e}_\phi$ is the unit vector in the toroidal direction.

As mentioned above, we use a setup derived from a study on the benign termination of RE beams in JET[12,13]. However, in contrast to Ref. 13, we do not include REs in our

[a)] Now at Indian Institute of Technology Guwahati, 781039, Assam, India

model. The toroidal field is 3.5 T at the geometric major radius $R_0 = 2.6$ m, giving $F_0 = 9.0$ T.m, and the plasma current $I_p = 0.75$ MA. The plasma has a nearly circular cross-section with a minor radius of 67 cm. As can be seen in Fig. 1, the initial j_ϕ and safety factor (q) profiles are non-monotonic. There are two $q = 4$ surfaces in the plasma and the $m/n = 4/1$ DTM is unstable (m and n are the poloidal and toroidal mode numbers). Fig. 2 shows profiles of the helical flux $\psi_* \equiv \int (1/q - 1/4) d\Psi_n$, where Ψ_n is the toroidal magnetic flux normalized between 0 and 1, for the initial equilibrium (plain line) and after the reconnection event (dashed line) as predicted by the Kadomtsev model generalized to the DTM[1,10]. One can see that the predicted reconnection region (i.e. the region where the radial coordinate, chosen here to be the square root of the normalized poloidal magnetic flux $\psi_n^{1/2}$, is a multiple-valued function of the initial ψ_*) extends from almost the very centre up to the edge of the plasma. We note that the proximity to the edge of the outer $q = 4$ surface is a key factor allowing the predicted reconnection region to extend up to the edge. Another, less trivial, contributing factor is that the plasma is in a limiter configuration. If it was instead in a divertor configuration, the divergence of q to infinity at the edge would result in a sharper variation of ψ_* and possibly in the predicted reconnection region not extending up to the edge (on the other hand, the large magnetic shear would promote island overlap, which might 'compensate').

Simulations are of the 'fixed boundary' type: Dirichlet boundary conditions are applied to ψ ($= \psi(t = 0)$), u, ω and j_ϕ (the latter three being set to 0). The fact that ψ is fixed at the boundary implies that magnetic perturbations go to 0 there. This probably explains why, in spite of the fact that q at the edge is very close to 5 (see Fig. 1), the $5/1$ mode seems to play a negligible role.

In the poloidal plane, Bézier finite elements are used[17] with a flux-surface-aligned grid comprising 7680 cells (120 radial by 64 poloidal). A Fourier representation is used in the toroidal direction, and harmonics $n = 0 - 15$ are resolved.

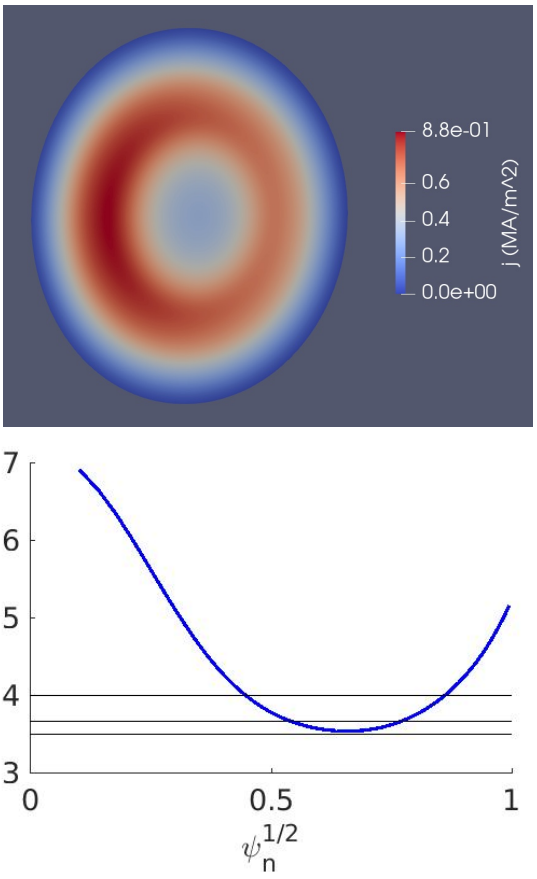

FIG. 1. Cross-section of the initial current density $j_{\phi 0}$ (top) and initial q profile (bottom). The horizontal lines in the right plot correspond, from top to bottom, to $q = 4$, $11/3$, and $7/2$. ψ_n is the poloidal magnetic flux normalized between 0 and 1.

III. VIOLENT RELAXATION AT $\eta = 10^{-6}$

We first describe a simulation with $\eta = \mu = 10^{-6}$, in which we observed a violent relaxation. Note that these η and μ values are normalized. The corresponding values in SI units are $\eta_{SI} = \sqrt{\mu_0/\rho} \cdot \eta \simeq 6.1 \cdot 10^{-6}$ Ω.m, which is equal to the Spitzer resistivity[14] at 27 eV, and $\mu_{SI} = \sqrt{\mu_0/\rho} \cdot \mu / R^2 \simeq 9.0 \cdot 10^{-7}$ kg/m/s, which corresponds to a momentum diffusivity of 27 m^2/s. Fig. 3 shows j_ϕ and Poincaré cross-sections (left) and u cross-sections (right) at different times. It can be seen that in the first few ms, two 4/1 island chains grow around the $q = 4$ surfaces (second row, $t = 3.62$ ms). After some time, island overlap results in the stochastization of the magnetic field over a broad region in which small scale structures appear, while intact flux surfaces remain in the core (third row, $t = 4.30$ ms). Shortly after this, a strong macroscopic $4/1$ flow develops in the stochastic region, which violently 'stirs' the plasma (fourth row, $t = 4.35$ ms). A region with still intact flux surfaces remains in the core (at the edge of which a skin

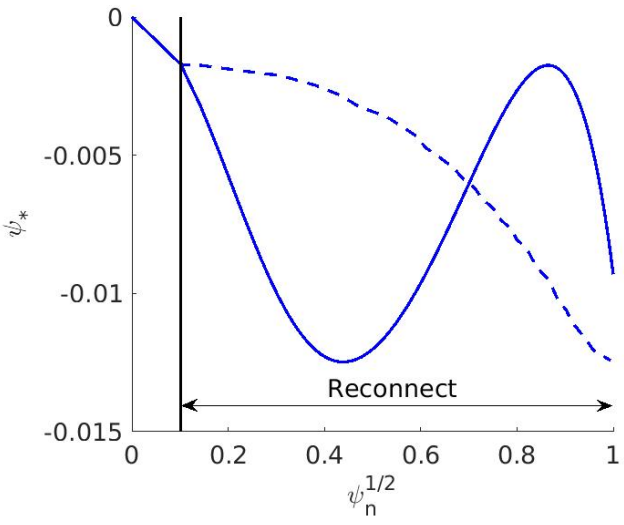

FIG. 2. Profiles of the helical flux ψ_* for the initial equilibrium (plain line) and after the reconnection event (dashed line) as predicted by the Kadomtsev model.

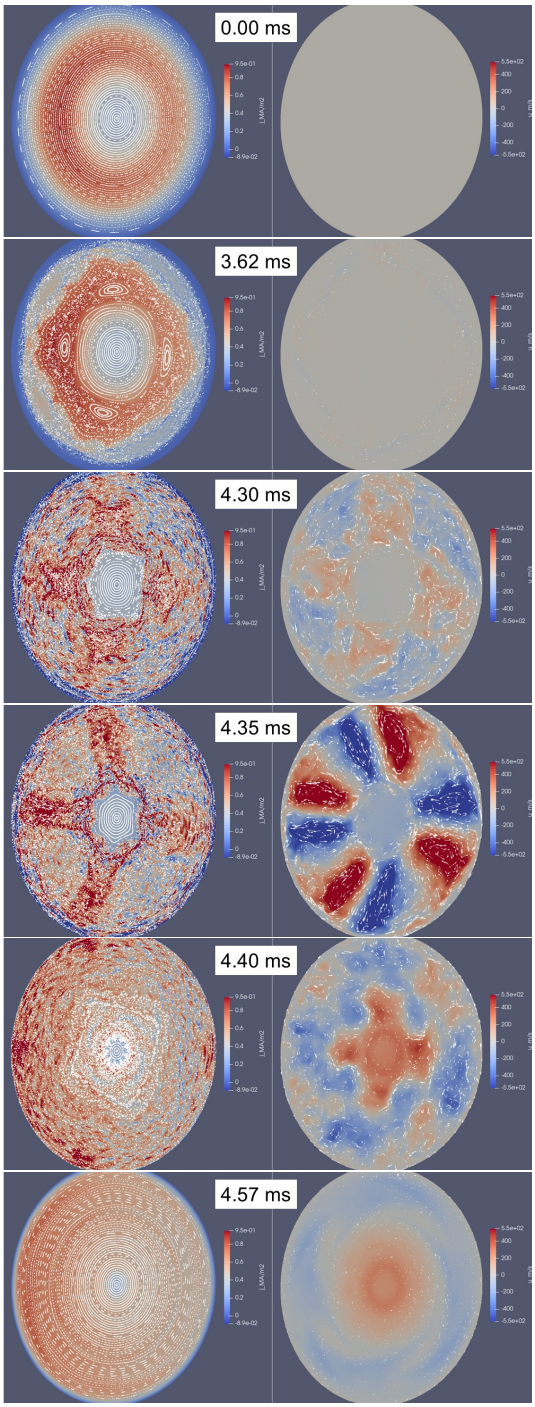

FIG. 3. j_ϕ and Poincaré cross-sections (left) and electric/flow potential cross-sections together with arrows indicating the direction and magnitude of the flow (right) for the simulation with $\eta = 10^{-6}$ at different times.

current is visible) but this region shrinks in time, until eventually all flux surfaces are destroyed. Subsequently, the flow decays, j_ϕ tends to homogenize, and flux surfaces promptly reform (fifth and sixth rows, $t = 4.40$ and 4.57 ms).

Fig. 4 shows the evolution of the plasma current I_p (blue), internal inductance l_{i3} (red), energy in the n=0 component

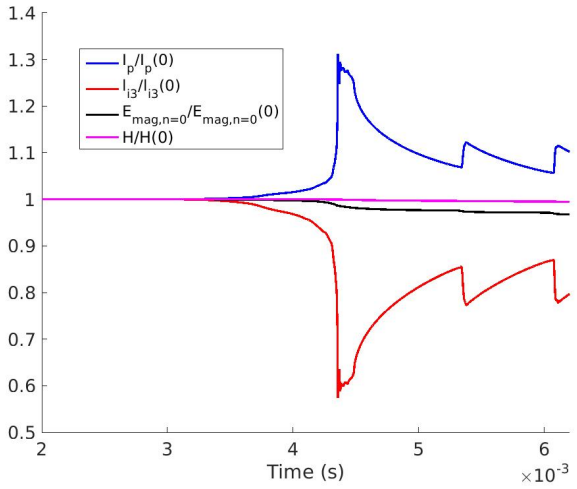

FIG. 4. Evolution of the plasma current I_p, internal inductance l_{i3}, energy in the n=0 component of the magnetic field $E_{mag,n=0}$, and volume-integrated magnetic helicity H, each normalized to their initial value, for the simulation with $\eta = 10^{-6}$.

of the magnetic field $E_{mag,n=0}$ (black), and volume-integrated magnetic helicity $H \equiv \int \mathbf{A}\cdot\mathbf{B}dV$ (where $\mathbf{A}$ is the vector potential and $\mathbf{B}$ the magnetic field) (magenta), each normalized to their initial value. A large I_p spike is visible at 4.36 ms, followed by smaller spikes at 5.35 and 6.08 ms. The first spike corresponds to the violent relaxation described above. It is accompanied by a strong drop of l_{i3} and by the release of a small amount of magnetic energy. The helicity remains almost constant, as expected from the theory of fast MHD relaxations[18]. Details regarding the calculation and conservation of H in our model are given in Appendix A. The subsequent I_p spikes are due to further, smaller, relaxations which take place due to the fact that the $\eta(j_\phi - j_{\phi 0})$ term in Eq. 1 drives the system back to an unstable state.

IV. RESISTIVITY DEPENDENCE OF THE NON-LINEAR BEHAVIOUR

We now investigate the effect of η on the dynamics. Figure 5 shows the evolution of I_p for different values of η. Note that this η scan is performed at constant magnetic Prandtl number, keeping $\mu = \eta$. However, an η scan at fixed μ produces qualitatively similar results. A general remark on Figure 5 is that, not surprisingly, the dynamics are faster at larger η. Then, as we saw above, a large I_p spike is observed for $\eta = 10^{-6}$. This is also the case for somewhat higher and lower resistivity: $\eta = 3\cdot 10^{-6}$ and $5\cdot 10^{-7}$, corresponding to the Spitzer resistivity at 13 and 47 eV respectively. However, in the latter case, i.e. going in the direction of lower η, one can observe first a moderate rise in I_p (from 0.75 to 0.77 MA) followed by a plateau and only then a large I_p spike. In the cases with lower η still ($\eta = 3\cdot 10^{-7}$ and 10^{-7}), only the moderate I_p rise and some part of the ensuing plateau are visible. Simulations have not been pushed further because they are very expensive

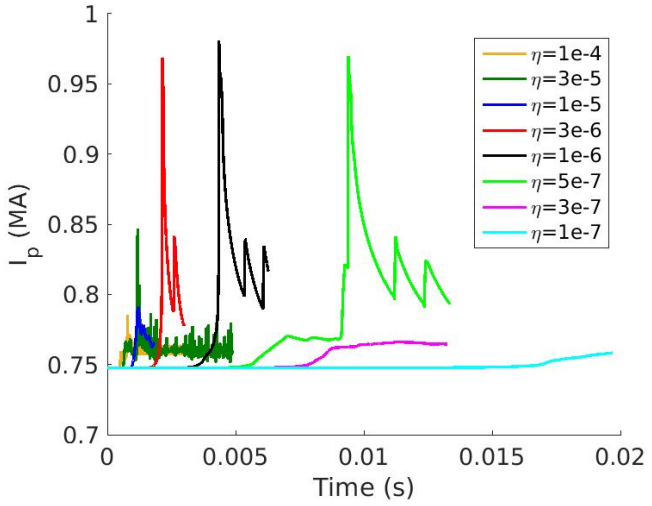

FIG. 5. Evolution of I_p for different values of the resistivity η. A large I_p spike, indicative of a global relaxation, can be seen at $\eta = 3\cdot10^{-6}$, 10^{-6} and $5\cdot10^{-7}$, but not at other values. Note that the cases with $\eta = 3\cdot10^{-7}$ and 10^{-7} have not been pushed further because they are very expensive in computing time, so it is not known for sure whether a large I_p spike would arise later. However, Fig. 6 suggests that this would not be the case (at least for the $\eta = 3\cdot10^{-7}$ case) because magnetic energies in the different toroidal Fourier modes seem to have saturated by the end of the simulation.

in computing time, so it is not known whether a large I_p spike would happen later. Still, the behaviour observed for the lower η values contrasts with the 'straight' large I_p spike observed at intermediate η values (10^{-6} and $3\cdot10^{-6}$). We will investigate the reasons in Section IV A by comparing the cases $\eta = 10^{-6}$ and $\eta = 3\cdot10^{-7}$. If we now turn our attention to the higher η cases (10^{-5}, $3\cdot10^{-5}$ and 10^{-4}) on Figure 5, we can observe that the I_p spike is much smaller (the term 'spike' may actually not be fully adequate). We will investigate the reason in Section IV B.

A. Comparison between cases $\eta = 10^{-6}$ and $\eta = 3\cdot10^{-7}$

Let us now compare the cases $\eta = 10^{-6}$ and $\eta = 3\cdot10^{-7}$. Looking at the time evolution of the volume-integrated magnetic energies in the toroidal harmonics $n = 1-5$, shown in Fig. 6 for $\eta = 10^{-6}$ (top) and $\eta = 3\cdot10^{-7}$ (bottom), it appears that the early evolution is similar for the two cases, although slower for the lower η case, as expected. This early evolution begins with a quasi-linear growth of the 4/1 DTM which lasts up to the time when the $n = 1$ magnetic energy, $E_{mag,n=1}$, reaches $\simeq 10^{-6}$. We precise *quasi*-linear because during this phase, higher-order harmonics grow as a result of the beating of lower-order harmonics (e.g. $n = 1+n = 1 \rightarrow n = 2$, $n = 1+n = 2 \rightarrow n = 3$ etc., with growth rates adding up, like described e.g. in Section IV.A of Ref. 19), without affecting the growth of the $n = 1$ mode. After this, the DTM is in the non-linear so-called 'Rutherford' phase[18]. It is interesting to

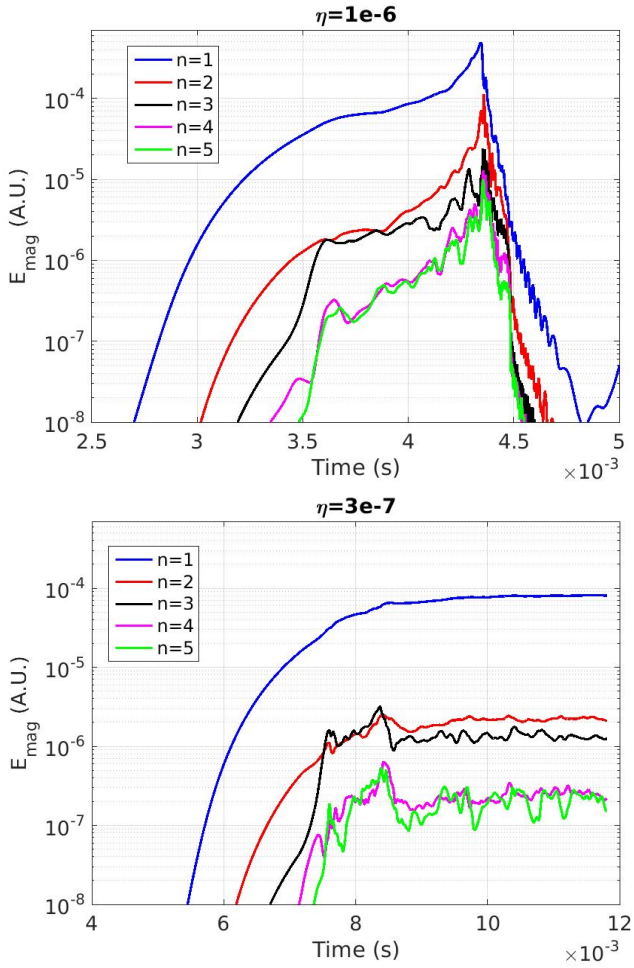

FIG. 6. Evolution of the magnetic energy in the toroidal harmonics $n = 1-5$ for $\eta = 10^{-6}$ (top) and $\eta = 3\cdot10^{-7}$ (bottom).

see that if we plot the energies for the case $\eta = 3\cdot10^{-7}$ as a function of a rescaled time $t' = t/3.3 + 1.13$ ms, where the factor 3.3 corresponds to the resistivity ratio, the two cases have a very similar evolution for the $n = 1$ and $n = 2$ harmonics during the Rutherford phase, as shown in Fig. 7. Indeed, from theory it is expected that the dynamics should be invariant by a transformation of the type $t \rightarrow \alpha t$, $\eta \rightarrow \eta/\alpha$ during this phase (the island width w grows at a rate $dw/dt \propto \eta$).

However, while the $n = 1$ and $n = 2$ energies are closely matched, it can be seen in Fig. 7 that the $n = 3$ mode (in black) grows earlier and faster (in terms of the rescaled time t') for the $\eta = 3\cdot10^{-7}$ case. From the cross-section of the $n = 3$ component of the poloidal magnetic flux ψ, shown in Fig. 8 at 3.40 ms (rescaled time) for the simulation at $\eta = 3\cdot10^{-7}$, it can be seen that the $n = 3$ mode is an $11/3$ tearing mode.

Fig. 9 compares the two cases at 3.40 ms (still using the rescaled time for the $\eta = 3\cdot10^{-7}$ case). At this time, as can be seen in Fig. 7, the $11/3$ mode has already grown substantially for the $\eta = 3\cdot10^{-7}$ case but not for the $\eta = 10^{-6}$ case, and Fig. 9 shows that the $11/3$ mode has generated magnetic stochasticity at the edge of the outer $4/1$ island.

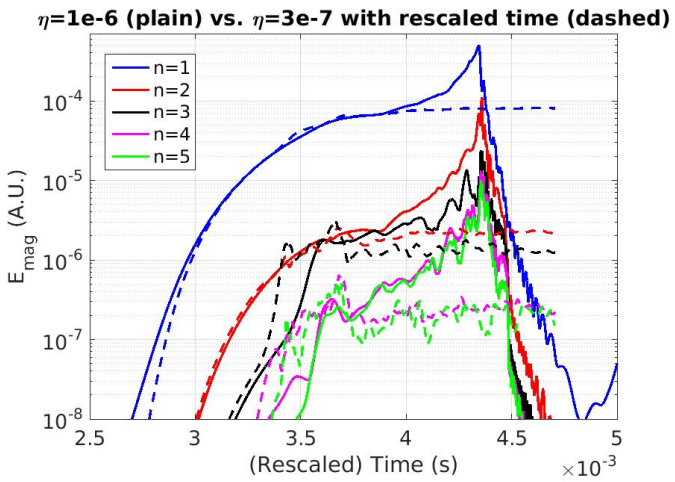

FIG. 7. Same as Fig. 6 but overlaying $\eta = 10^{-6}$ (plain) and $\eta = 3\cdot10^{-7}$ (dashed) and using a rescaled time for the case $\eta = 3\cdot10^{-7}$, like explained in the text.

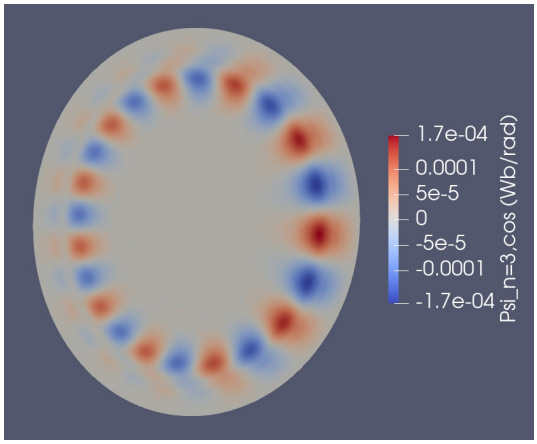

FIG. 8. Poloidal cross-section of the $n = 3$ (cosine) component of the poloidal magnetic flux ψ at 3.40 ms (rescaled time) in the simulation at $\eta = 3\cdot10^{-7}$.

What drives the $11/3$ mode is likely the radial gradient of j_ϕ at the edge of the outer $4/1$ magnetic island. Indeed, in the Rutherford regime, j_ϕ (or more precisely j_ϕ/B) tends to be constant on (helical) flux surfaces inside the island[18], and this generates a substantial j_ϕ radial gradient near the edge of the island, as can be seen in Fig. 10, which shows j_ϕ profiles along the white line visible in Fig. 9. The blue profiles are taken at equivalent times for the $\eta = 10^{-6}$ (plain) and $\eta = 3\cdot10^{-7}$ (dashed) simulations, shortly before the growth of the $11/3$ mode. A large j_ϕ gradient is visible at a radial coordinate $\simeq 0.57$ m. The remarkable similarity between these profiles is a consequence of the fact that the dynamics have up to that time been dominated by the growth of the $4/1$ DTM in the Rutherford regime for both simulations. On the other hand, the red profiles, which are taken slightly later (and once again at equivalent times), are clearly different because the $11/3$ mode has now grown in the $\eta = 3\cdot10^{-7}$ simulation, leading to magnetic stochasticity (as visible in Fig. 9) and to a wiggly j_ϕ profile, while it has not yet grown in the $\eta = 10^{-6}$ simulation. The reason why the $11/3$ mode grows relatively faster in the $\eta = 3\cdot10^{-7}$ simulation is most likely that its growth starts in the linear regime, where the growth rate scales like[18] $\eta^{3/5}$, whereas the $4/1$ mode is already in the Rutherford regime, where its characteristic evolution rate scales like η. Thus, the growth rate of the $11/3$ mode *relative to* the characteristic evolution rate of the $4/1$ mode scales like $\eta^{-2/5}$ and is thus larger at smaller η. Note that this effect may actually be reinforced by the fact that at large η the linear tearing mode growth rate is smaller than suggested by the $\eta^{3/5}$ scaling due to finite resistive layer width effects (see e.g. Fig. 2 in Ref. 20). A possible further factor could be the existence of a critical Δ' for linear tearing mode growth due to the finite viscosity and resistivity, which is larger at larger resistivity[21]. However, it appears unlikely that this plays a significant role since this critical Δ' theoretically scales as $\eta^{1/6}\mu^{1/6}$ and thus differs by only about 20 % between the two cases $\eta = 10^{-6}$ and $\eta = 3\cdot10^{-7}$. Furthermore, we have repeated the simulation at $\eta = 10^{-6}$ with a 10 times lower viscosity, which should more than compensate the effect of η on the critical Δ', and found almost no effect on the growth of the $11/3$ mode.

Even though, as mentioned above, it is not known whether the $\eta = 3\cdot10^{-7}$ case would produce a violent relaxation if pushed further in time, it can be seen in Fig. 7 that the magnetic energies in the various toroidal harmonics remain almost constant in time after 4 ms (rescaled time), suggesting that some kind of 'gentle saturation' has occurred. This is likely a consequence of the mild stochastization generated by the growth of the $11/3$ mode, which presumably affects the j_ϕ distribution in such a way as to reduce the drive for other modes involved in the violent relaxation. To be more precise, an investigation of the simulation with $\eta = 10^{-6}$ reveals that the violent relaxation is initiated by the growth of a secondary $7/2$ mode at about 4 ms (corresponding to the growth of the $n = 2$ magnetic energy visible in Fig. 6 (top)). This mode boosts magnetic stochasticity and presumably acts as a 'magnetic trigger'[22] leading to the fast macroscopic flow visible in Fig. 3 (fourth row) and to the associated violent relaxation. The $7/2$ mode appears to be excited by the radial j_ϕ gradient developing near the $q = 7/2$ surface as the $4/1$ islands grow. However, in the $\eta = 3\cdot10^{-7}$ case, because of the stochasticity generated by the $11/3$ mode, the j_ϕ profile starts relaxing early on, which reduces the excitation of the $7/2$ mode. This seems like a plausible explanation for the absence of a fast relaxation in this simulation.

Two 'numerical experiments' support this picture. First, if we begin a simulation with $\eta = 10^{-6}$ and reduce η to $3\cdot10^{-7}$ at 3.83 ms, i.e. after the large j_ϕ gradient has passed across the $q = 11/3$ surface, we observe a large I_p spike. This is shown in Figure 11. Second, if we include only the toroidal harmonics $n = 0-2$ in the simulations, thus removing the $11/3$ mode, simulations at $\eta = 10^{-6}$ and $\eta = 3\cdot10^{-7}$ behave much more similarly, as shown in Figure 12 (note that none of them produces a violent relaxation, but this is probably because $n \geq 3$ harmonics are required for that).

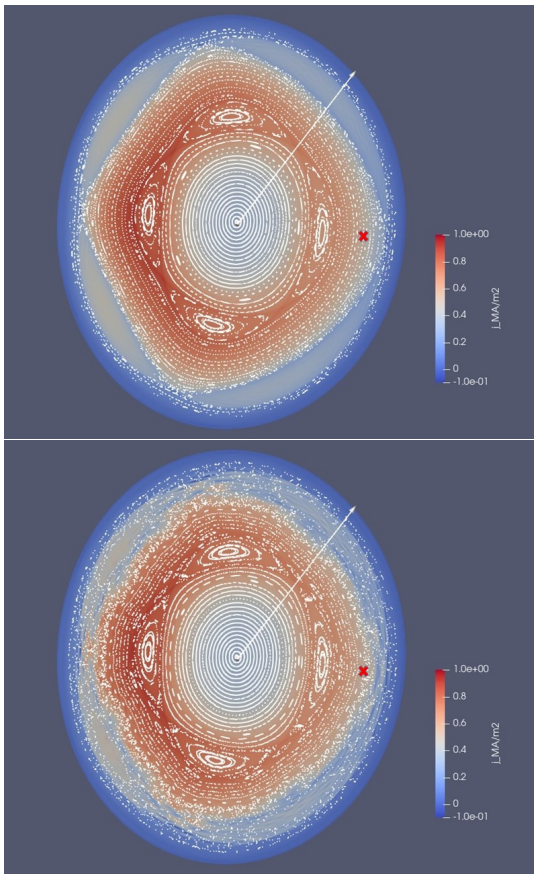

FIG. 9. j_ϕ and Poincaré cross-sections for $\eta = 10^{-6}$ at 3.40 ms (top) and for $\eta = 3 \cdot 10^{-7}$ at $t = 7.49$ ms (i.e. $t' = 3.40$ ms) (bottom). Profiles shown in Fig. 10 are taken along the white line. The red cross indicates the position of the $q = 11/3$ surface.

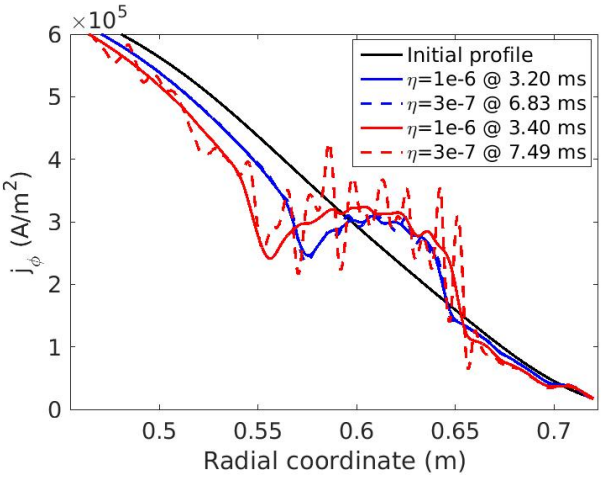

FIG. 10. j_ϕ profiles taken along the white line shown in Fig. 9 for $\eta = 10^{-6}$ (plain) and $\eta = 3 \cdot 10^{-7}$ (dashed). Identical colours indicate equivalent times.

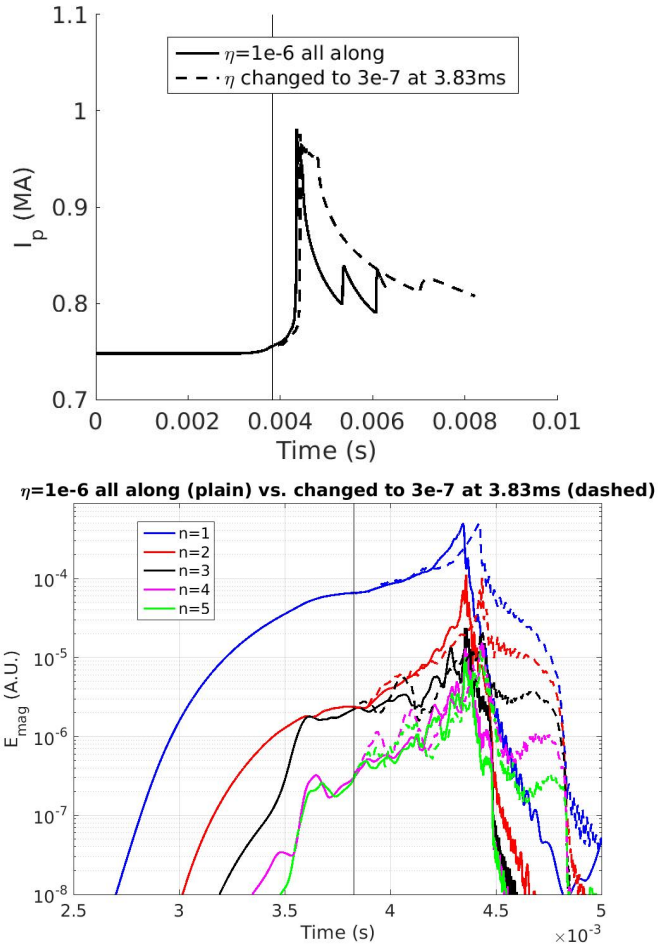

FIG. 11. Comparison between the simulation at $\eta = 10^{-6}$ (plain lines) and a simulation started with $\eta = 10^{-6}$ but reducing η to $3 \cdot 10^{-7}$ at 3.83 ms (dashed lines). Note that no time rescaling is applied here.

B. Analysis of high η cases

We now discuss why the high η cases ($\eta = 10^{-5}$, $3 \cdot 10^{-5}$ and 10^{-4}) do not display a violent relaxation. Although it is difficult to identify the reasons in detail, this is likely again related to how fast secondary modes grow with respect to the primary mode, but this time the relevant secondary mode is the $7/2$ mode. We mentioned above the key role that this mode appears to play in the fast relaxation observed at $\eta = 10^{-6}$. In the simulation at $\eta = 10^{-5}$, no large growth of the $7/2$ mode is observed. It can indeed be seen in Fig. 13 (which is the same as Fig. 7 but now also including the case $\eta = 10^{-5}$, for which we have rescaled time in the following 'Rutherford-like' way: $t'' = 10 \cdot t - 6.3$ ms) that the behaviour of the magnetic energies is much smoother at $\eta = 10^{-5}$ than at $\eta = 10^{-6}$, with no fast growth of the $n = 2$ energy in the former case (one might notice that, on the other hand, the $n = 2$ energy is larger for a short period of time in the $\eta = 10^{-5}$ case; however, it should be kept in mind that the energies plotted here are summed over all poloidal harmonics, and detailed inspection reveals

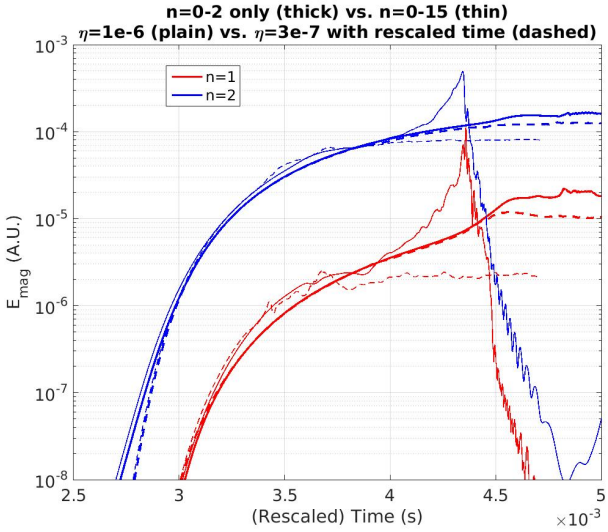

FIG. 12. Evolution of the magnetic energy in the $n = 1$ and $n = 2$ toroidal harmonics in simulations including only $n = 0-2$ (thick lines) or $n = 0-15$ (thin lines) and for $\eta = 10^{-6}$ (plain lines) and $\eta = 3 \cdot 10^{-7}$ (dashed lines) with, in the latter case, a time rescaling like already used above ($t' = t/3.3 + 1.13$ ms).

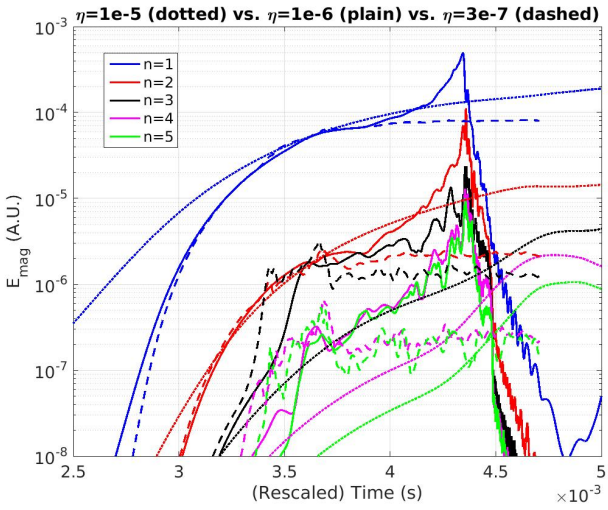

FIG. 13. Same as Fig. 7 but now also including the case $\eta = 10^{-5}$.

that this is not related to the $7/2$ mode). The absence of a large growth of the $7/2$ mode at $\eta = 10^{-5}$ is consistent with secondary modes growing more slowly with respect to the primary mode at higher η, which is reminiscent of the discussion about the $11/3$ mode in Section IV A.

The difference in magnetic stochasticity between the $\eta = 10^{-5}$ and $\eta = 10^{-6}$ cases is visible in Fig. 14, which shows Poincaré cross-sections for $\eta = 10^{-5}$ (top row) and $\eta = 10^{-6}$ (bottom row) at 3.5 ms (left column) and 4.2 ms (right column), using the above-mentioned time rescaling for the $\eta = 10^{-5}$ case. It can be seen that at 3.5 ms, the distortion of magnetic surfaces is similar in the two simulations, as evidenced by the green line which is copy-pasted from the $\eta = 10^{-5}$ plot (top left) into the $\eta = 10^{-6}$ plot (bottom left). However, already at this time more stochasticity is visible in the lower η case. This is consistent to what we saw in Section IV A when comparing simulations at $\eta = 10^{-6}$ and $\eta = 3 \cdot 10^{-7}$. At 4.2 ms (right plots), the difference in stochasticity has increased dramatically, with almost complete stochasticity in the region $\psi_n^{1/2} \geq 0.3$ at $\eta = 10^{-6}$ while flux surfaces remain at $\eta = 10^{-5}$. A large stochastic region like in the $\eta = 10^{-6}$ is in fact never observed at any time in the $\eta \geq 10^{-5}$ simulations. In the absence of such a 'magnetic trigger', it is not very surprising that the non-linear behaviour is different in these cases, although understanding this behaviour in detail and why a large I_p spike is not produced is beyond the scope of this paper.

V. SUMMARY AND DISCUSSION

In summary, our analysis has shown that the non-linear dynamics of the DTM depend on the resistivity η. The underlying mechanism appears related to secondary tearing modes which are non-linearly destabilized by the large j_ϕ gradient at the edge of the external $4/1$ island, which passes across other rational surfaces ($q = 11/3$ and $q = 7/2$ in particular) as the island grows. The key point is that these secondary modes grow faster *relative to* the primary mode when η is lower. These secondary modes play an important role in the non-linear dynamics, probably because they generate magnetic stochasticity. Indeed, while simulations at very large η ($\geq 10^{-5}$) exhibit only limited stochasticity, simulations at lower η ($3 \cdot 10^{-6} \geq \eta \geq 5 \cdot 10^{-7}$) are characterized by strong stochastization over eventually the whole domain as a result of the growth of the $7/2$ mode. A violent relaxation promptly follows. This connects to the topic of the 'magnetic trigger' discussed in Ref. 22 and more generally of the relation between reconnection and stochasticity in 3D situations, addressed in Ref. 19 and which is at the centre of a new paradigm for fast reconnection proposed by Boozer (see Ref. 23 and references therein). The relaxation leads to an almost complete flattening of the j_ϕ/B profile at fixed magnetic helicity H, resulting in a large I_p spike. This global character of the relaxation is consistent with the 'Kadomtsev-predicted' reconnection region extending from almost the very centre up to the edge of the plasma. Simulations with even lower η ($\leq 3 \cdot 10^{-7}$) do not produce such a violent relaxation. This appears to be due to the stronger growth of the $11/3$ mode in these cases and the early but localized stochasticity that it generates, which presumably causes a 'gentle relaxation' of the j_ϕ profile, cutting the drive for a subsequent growth of the $7/2$ mode.

The identification of these different non-linear behaviours depending on η may be of interest in the frame of understanding the termination of RE beams. The benign termination observed in recent experiments[13,24] after a deuterium injection into the beam seems related to the growth of an MHD mode up to a very large amplitude. In contrast, when high Z material is injected instead of deuterium, the MHD mode does not reach as large an amplitude. Based on the findings described

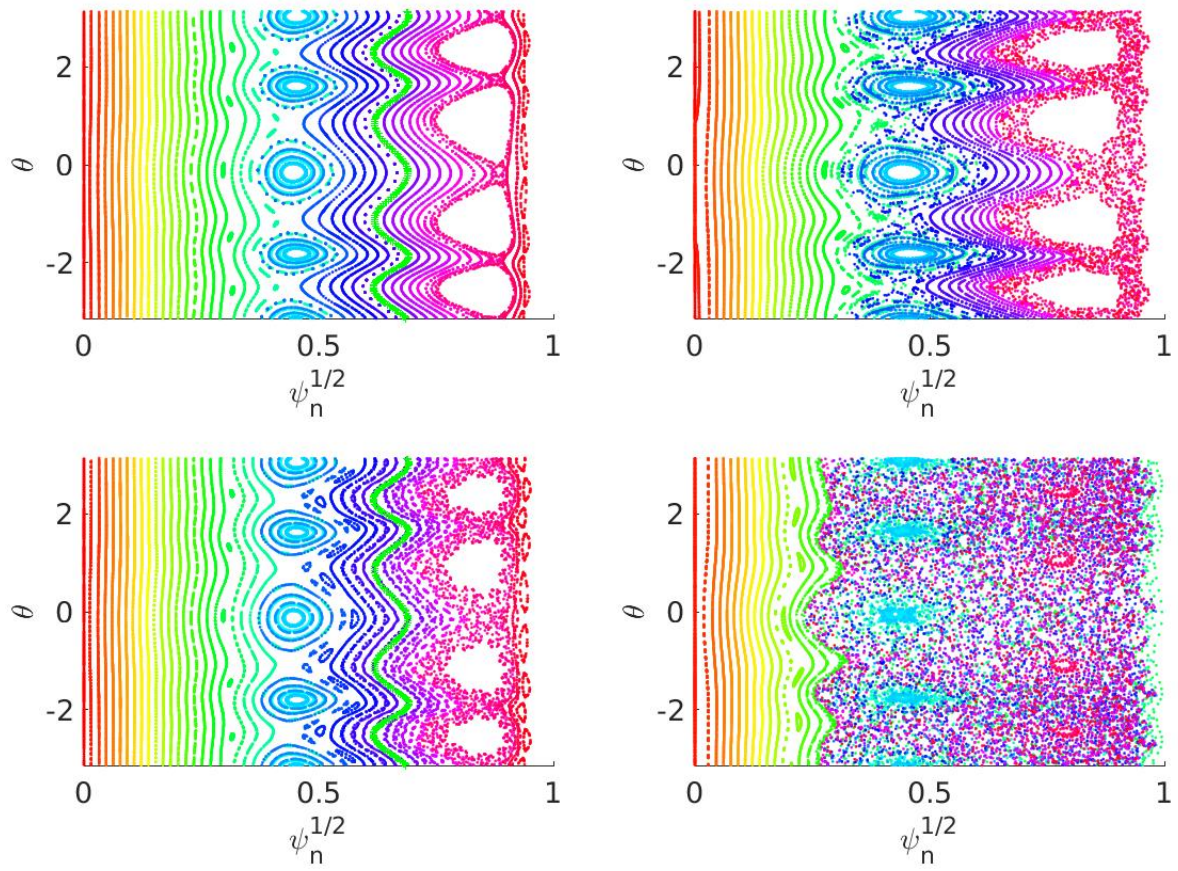

FIG. 14. Poincaré cross-sections for $\eta = 10^{-5}$ (top row) and $\eta = 10^{-6}$ (bottom row) at 3.5 ms (left column) and 4.2 ms (right column), using a rescaled time for the $\eta = 10^{-5}$ case ($t'' = 10 \cdot t - 6.3$ ms). Each colour corresponds to a different field line. The green line in the bottom left plot is copy-pasted from the green line in the top left plot to show that flux surface distortion is similar in the two simulations. ψ_n is the normalized poloidal flux and θ the poloidal angle.

in this paper, it may be hypothesized that this is related to a different resistivity of the background plasma. After a deuterium injection, the background plasma indeed appears to be colder (which can lead to recombination) than after a high Z injection (possibly because of an extra cooling channel provided by deuterium neutral transport[25]) and thus more resistive, with η probably reaching values higher still than 10^{-5} (i.e. higher than in the case discussed in Section IV B), which corresponds to the Spitzer resistivity at $\simeq 6$ eV. Based on the findings described in Section IV B, it may be hypothesized that this favors a growth of the main $(4/1)$ mode up to a larger amplitude before stochasticity appears and thus before the relaxation takes place, leading eventually to a more violent relaxation. In order to test this hypothesis, simulations starting earlier in time and including a self-consistent evolution of the current density profile and plasma geometry would be needed.

One caveat of our study is that REs were not included in the model. Helander et al. have investigated the impact of REs on the linear and non-linear properties of tearing modes[26]. A key finding was that *'the linear properties of the classical tearing mode are essentially determined by the cold bulk plasma, and the growth rate is approximately the same as in a plasma without runaways but with the same current profile'*. This suggests that our study, in spite of not including REs, has relevance for RE beam termination physics. There is one point to keep in mind, however, concerning our remark in Section IV A that the slower relative growth of secondary modes at higher η may actually be reinforced by the fact that at large η the linear tearing mode growth rate is smaller than suggested by the $\eta^{3/5}$ scaling: this should not apply when the current is carried by REs. Indeed, the deviation of the growth rate from the $\eta^{3/5}$ scaling results from a correction due to finite resistivity which, as discussed in Ref. 26, is actually absent when the current is carried entirely by REs. We plan in any case to include REs in future studies.

Another caveat is that, while the DTM may be relevant to (at least some) RE beam terminations at JET[13], in DIII-D (and also possibly in other JET cases) the relevant mode is instead thought to be the resistive external kink mode (typically associated to q reaching 2 at the edge of the plasma)[24,27]. However, non-linear simulation results show that the latter also involves the growth of primary and secondary magnetic islands (see e.g. Fig. 10 of Ref. 27), such that it is likely that the mechanisms discussed here are relevant also in this case.

ACKNOWLEDGMENTS

Simulations were run on the Marconi-Fusion supercomputer hosted at CINECA. This work has been carried out within the framework of the EUROfusion Consortium, funded by the European Union via the Euratom Research and Training Programme (Grant Agreement No 101052200 — EUROfusion). Views and opinions expressed are however those of the author(s) only and do not necessarily reflect those of the European Union or the European Commission. Neither the European Union nor the European Commission can be held responsible for them. Disclaimer: ITER is the Nuclear Facility INB no. 174. This paper explores physics processes during the plasma operation of the tokamak when disruptions take place; nevertheless the nuclear operator is not constrained by the results of this paper. The views and opinions expressed herein do not necessarily reflect those of the ITER Organization.

DATA AVAILABILITY STATEMENT

The data that support the findings of this study are available from the corresponding author upon reasonable request.

Appendix A: Expression and conservation theorem for the helicity

The expression for the magnetic field $\mathbf{B}$ corresponding to the reduced MHD model used in this work is:

$$\mathbf{B} = \nabla\psi \times \nabla\phi + F_0 \nabla\phi. \tag{A1}$$

An acceptable expression for the vector potential (i.e. one that satisfies $\mathbf{B} = \nabla \times \mathbf{A}$) is:

$$\mathbf{A} = \psi \nabla\phi - F_0 \frac{Z}{R} \nabla R. \tag{A2}$$

It is then easy to show that $\mathbf{A}\cdot\mathbf{B} = \frac{F_0}{R^2}(\psi - Z\partial_Z\psi)$. This is in practice the expression which is integrated over the simulation volume to calculate $H \equiv \int \mathbf{A}\cdot\mathbf{B} dV$.

Let us now consider dH/dt:

$$\begin{aligned} dH/dt = & \int \frac{F_0}{R^2} \partial_t (\psi - Z\partial_Z\psi) d\phi dS \\ = & \int \frac{F_0}{R^2} [2\partial_t\psi - \partial_Z(Z\partial_t\psi)] d\phi dS \end{aligned} \tag{A3}$$

where dS is an infinitesimal surface element in the poloidal plane. The second term in this integral can be readily integrated along Z to give boundary terms which vanish if $\partial_t\psi = 0$ at the boundary, which is the case here. The first term can be calculated by plugging in Eq. 1, i.e. $\partial_t\psi = R[\psi,u] - F_0\partial_\phi u + \eta(j_\phi - j_{\phi 0})$. The term involving $\partial_\phi u$ vanishes upon integration over ϕ and the term involving the Poisson bracket $[\psi,u]$ vanishes upon integration in the poloidal plane if $u = 0$ at the boundary, which is the case here. One is thus left with:

$$dH/dt = 2F_0 \int \frac{\eta(j_\phi - j_{\phi 0})}{R} d\phi dS, \tag{A4}$$

thus recovering the classical result that helicity is dissipated at a resistive rate only[18].

[1] B. Carreras, H. Hicks, and B. Waddell, "Tearing-mode activity for hollow current profiles," Nuclear Fusion **19**, 583 (1979).
[2] P. L. Pritchett, Y. C. Lee, and J. F. Drake, "Linear analysis of the double-tearing mode," The Physics of Fluids **23**, 1368–1374 (1980), https://aip.scitation.org/doi/pdf/10.1063/1.863151.
[3] D. Biskamp, *Magnetic Reconnection in Plasmas*, Cambridge Monographs on Plasma Physics (Cambridge University Press, 2000).
[4] Y. Ishii, M. Azumi, and Y. Kishimoto, "Structure-driven nonlinear instability of double tearing modes and the abrupt growth after long-time-scale evolution," Phys. Rev. Lett. **89**, 205002 (2002).
[5] C. L. Zhang and Z. W. Ma, "Nonlinear evolution of double tearing mode with guiding magnetic field," Physics of Plasmas **18**, 052303 (2011), https://doi.org/10.1063/1.3581064.
[6] M. Janvier, Y. Kishimoto, and J. Q. Li, "Structure-driven nonlinear instability as the origin of the explosive reconnection dynamics in resistive double tearing modes," Phys. Rev. Lett. **107**, 195001 (2011).
[7] T. Akramov and H. Baty, "Non-linear growth of double tearing mode: Explosive reconnection, plasmoid formation, and particle acceleration," Physics of Plasmas **24**, 082116 (2017), https://doi.org/10.1063/1.5000273.
[8] W. Guo, J. Ma, and Z. Yu, "Multiple secondary islands formation in nonlinear evolution of double tearing mode simulations," Physics of Plasmas **24**, 032115 (2017), https://doi.org/10.1063/1.4978789.
[9] Z. X. Wang, X. G. Wang, J. Q. Dong, Y. A. Lei, Y. X. Long, Z. Z. Mou, and W. X. Qu, "Fast resistive reconnection regime in the nonlinear evolution of double tearing modes," Phys. Rev. Lett. **99**, 185004 (2007).
[10] P. Maget, G. T. A. Huysmans, X. Garbet, M. Ottaviani, H. Lütjens, and J.-F. Luciani, "Nonlinear magnetohydrodynamic simulation of tore supra hollow current profile discharges," Physics of Plasmas **14**, 052509 (2007), https://doi.org/10.1063/1.2733677.
[11] P. Maget, H. Lütjens, J.-F. Luciani, X. Garbet, O. Février, and J.-L. Ségui, "Bi-fluid and neoclassical effect on a double-tearing mode in tore supra," Physics of Plasmas **21**, 062504 (2014), https://doi.org/10.1063/1.4882259.
[12] C. Reux, C. Paz-Soldan, P. Aleynikov, V. Bandaru, O. Ficker, S. Silburn, M. Hoelzl, S. Jachmich, N. Eidietis, M. Lehnen, S. Sridhar, and J. contributors, "Demonstration of safe termination of megaampere relativistic electron beams in tokamaks," Phys. Rev. Lett. **126**, 175001 (2021).
[13] V. Bandaru, M. Hoelzl, C. Reux, O. Ficker, S. Silburn, M. Lehnen, N. Eidietis, J. Team, and J. Contributors, "Magnetohydrodynamic simulations of runaway electron beam termination in jet," Plasma Physics and Controlled Fusion **63**, 035024 (2021).
[14] J. Wesson, *Tokamaks; 4th ed.*, International series of monographs on physics (Oxford Univ. Press, Oxford, 2011).
[15] M. Hoelzl, G. Huijsmans, S. Pamela, M. Bécoulet, E. Nardon, F. Artola, B. Nkonga, C. Atanasiu, V. Bandaru, A. Bhole, D. Bonfiglio, A. Cathey, O. Czarny, A. Dvornova, T. Fehér, A. Fil, E. Franck, S. Futatani, M. Gruca, H. Guillard, J. Haverkort, I. Holod, D. Hu, S. Kim, S. Korving, L. Kos, I. Krebs, L. Kripner, G. Latu, F. Liu, P. Merkel, D. Meshcheriakov, V. Mitterauer, S. Mochalskyy, J. Morales, R. Nies, N. Nikulsin, F. Orain, J. Pratt, R. Ramasamy, P. Ramet, C. Reux, K. Särkimäki, N. Schwarz, P. S. Verma, S. Smith, C. Sommariva, E. Strumberger, D. van Vugt, M. Verbeek, E. Westerhof, F. Wieschollek, and J. Zielinski, "The jorek non-linear extended mhd code and applications to large-scale instabilities and their control in magnetically confined fusion plasmas," Nuclear Fusion **61**, 065001 (2021).
[16] G. Huysmans and O. Czarny, "Mhd stability in x-point geometry: simulation of elms," Nuclear Fusion **47**, 659 (2007).
[17] O. Czarny and G. Huysmans, "Bézier surfaces and finite elements for mhd simulations," Journal of Computational Physics **227**, 7423–7445 (2008).

[18]D. Biskamp, *Nonlinear Magnetohydrodynamics*, Cambridge Monographs on Plasma Physics (Cambridge University Press, 1993).
[19]D. Borgogno, D. Grasso, F. Porcelli, F. Califano, F. Pegoraro, and D. Farina, "Aspects of three-dimensional magnetic reconnection," Physics of Plasmas **12** (2005), 10.1063/1.1857912, 032309, https://pubs.aip.org/aip/pop/article-pdf/doi/10.1063/1.1857912/14722385/032309_1_online.pdf.
[20]F. Militello, G. Huysmans, M. Ottaviani, and F. Porcelli, "Effects of local features of the equilibrium current density profile on linear tearing modes," Physics of Plasmas **11**, 125–128 (2003), https://pubs.aip.org/aip/pop/article-pdf/11/1/125/12518563/125_1_online.pdf.
[21]D. Grasso, R. J. Hastie, F. Porcelli, and C. Tebaldi, "Critical Delta' for stability of viscoresistive tearing modes," Physics of Plasmas **15** (2008), 10.1063/1.2957916, 072113.
[22]A. Lichtenberg, K. Itoh, S.-I. Itoh, and A. Fukuyama, "The role of stochasticity in sawtooth oscillations," Nuclear Fusion **32**, 495 (1992).
[23]A. H. Boozer, "Magnetic reconnection and thermal equilibration," Physics of Plasmas **28** (2021), 10.1063/5.0031413, 032102, https://pubs.aip.org/aip/pop/article-pdf/doi/10.1063/5.0031413/13821059/032102_1_online.pdf.
[24]C. Paz-Soldan, C. Reux, K. Aleynikova, P. Aleynikov, V. Bandaru, M. Beidler, N. Eidietis, Y. Liu, C. Liu, A. Lvovskiy, S. Silburn, L. Bardoczi, L. Baylor, I. Bykov, D. Carnevale, D. D.-C. Negrete, X. Du, O. Ficker, S. Gerasimov, M. Hoelzl, E. Hollmann, S. Jachmich, S. Jardin, E. Joffrin, C. Lasnier, M. Lehnen, E. Macusova, A. Manzanares, G. Papp, G. Pautasso, Z. Popovic, F. Rimini, D. Shiraki, C. Sommariva, D. Spong, S. Sridhar, G. Szepesi, C. Zhao, the DIII-D Team, and J. Contributors, "A novel path to runaway electron mitigation via deuterium injection and current-driven mhd instability," Nuclear Fusion **61**, 116058 (2021).
[25]E. M. Hollmann, I. Bykov, N. W. Eidietis, J. L. Herfindal, A. Lvovskiy, R. A. Moyer, P. B. Parks, C. Paz-Soldan, A. Y. Pigarov, D. L. Rudakov, D. Shiraki, and J. Watkins, "Study of argon expulsion from the post-disruption runaway electron plateau following low-Z massive gas injection in DIII-D," Physics of Plasmas **27**, 042515 (2020), https://pubs.aip.org/aip/pop/article-pdf/doi/10.1063/5.0003299/15926175/042515_1_online.pdf.
[26]P. Helander, D. Grasso, R. J. Hastie, and A. Perona, "Resistive stability of a plasma with runaway electrons," Physics of Plasmas **14**, 122102 (2007), https://doi.org/10.1063/1.2817016.
[27]C. Liu, C. Zhao, S. C. Jardin, N. M. Ferraro, C. Paz-Soldan, Y. Liu, and B. C. Lyons, "Self-consistent simulation of resistive kink instabilities with runaway electrons," Plasma Physics and Controlled Fusion **63**, 125031 (2021).